Supplementary Figures and Extended Methods

Broadfield, Duarte, Schmieder et al. 2021: **Fat induces glucose metabolism in non-transformed liver cells and promotes liver tumorigenesis**

Supplementary Figures

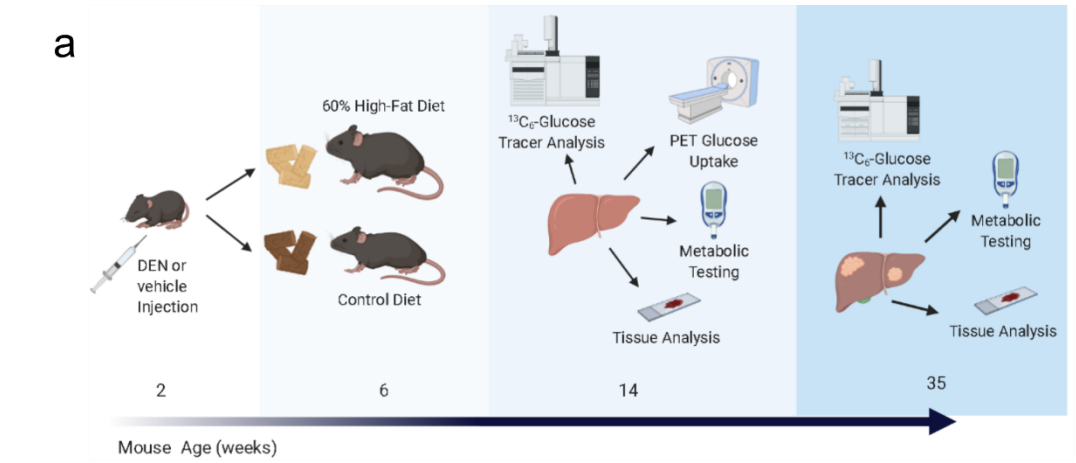

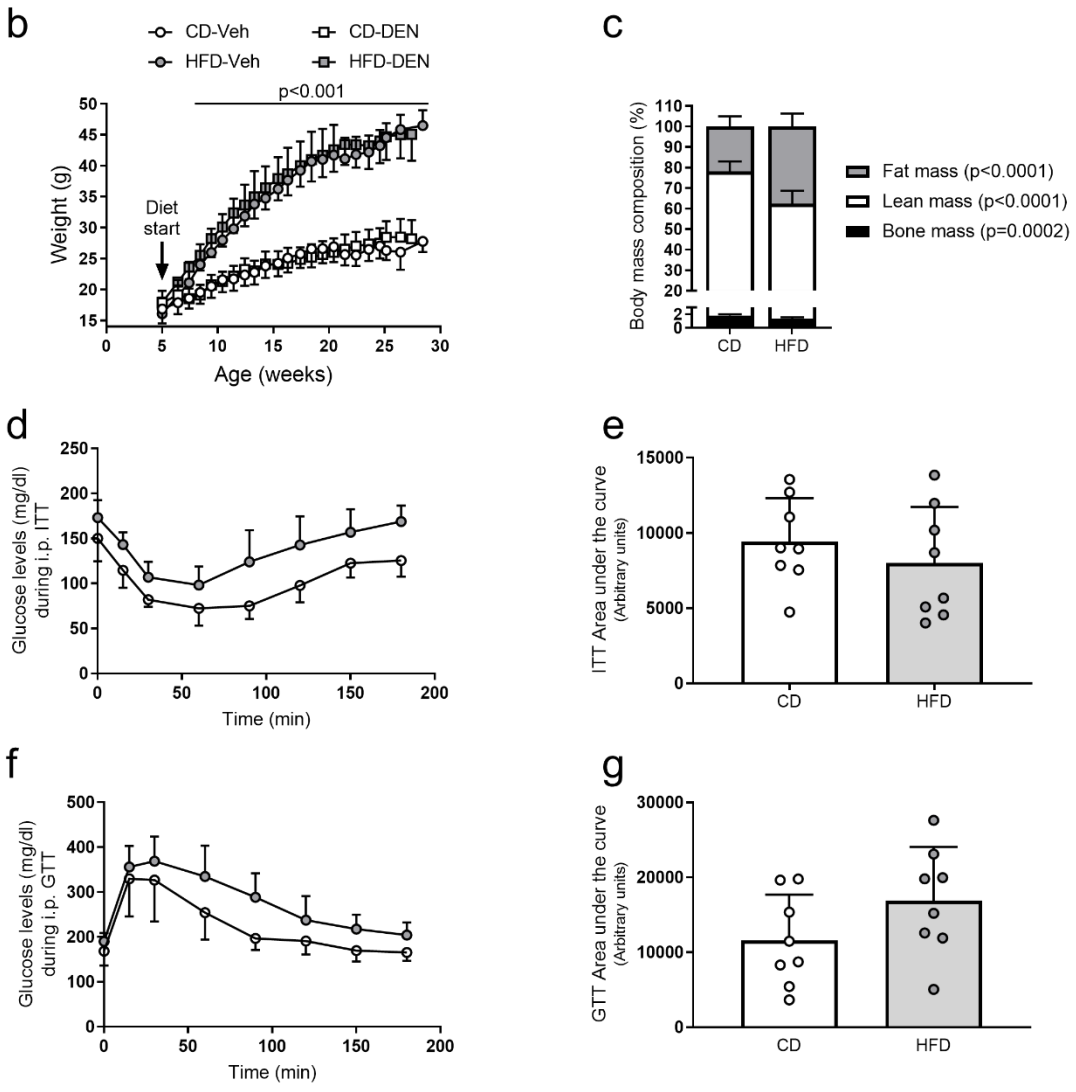

Supplementary Figure 1: Effect of 8-weeks of high fat diet feeding on whole body physiology.

a) Simplified schematic overview of the experimental setup used for in vivo experiments. Briefly, 2-week old male C57/BL6N mice were injected with either 25 mg/kg diethylnitrosamine (DEN) or phosphate buffered saline (vehicle, Veh). At 6-weeks of age, mice were then subdivided into two groups, one receiving a high fat diet and the other a control diet. At 14- and 35-weeks of age (8- and 29-weeks on the diets, respectively) mice underwent a $^{13}C_6$-glucose tracer infusion for a period of approximately 6-hours to determine their hepatic metabolism.

b) Mouse weight on high fat (HFD) or control (CD) diet over the course of the experiment (n≥8).

c) Dual X-ray absorptiometry (DEXA) performed on mice fed a control (CD-vehicle; n=8) or high fat (HFD-vehicle=8) diet for 8-weeks. p-values for comparing CD to HFD are as indicated in the legend for each tissue type. Data are averages ± standard deviation.

d-g) Intraperitoneal insulin (i.p. ITT, 1 unit/kg body weight) and glucose (i.p. GTT, 2 mg/kg body weight) tolerance test performed on mice after 8-weeks on a control diet (CD-vehicle; n=8) or high fat (HFD-vehicle=8), and is represented by the change in blood glucose levels (mg/dL) and area under the curve.

Data for all figures is average ± standard deviation. Statistics: two-way ANOVA (panel b) and two-tailed unpaired Student's t-test (remaining panels).

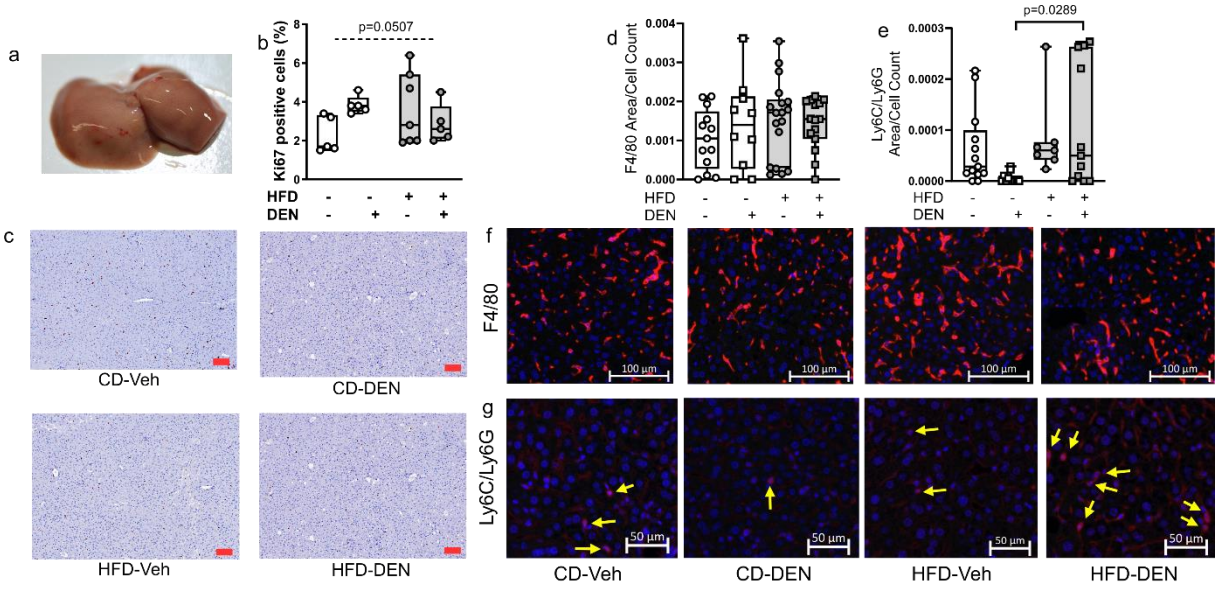

Figure S2: Mouse livers are normal in respect to hepatocarcinogenesis after 8-weeks of control or high fat diet.

a) Representative image of a mouse liver after 8-weeks on high fat diet.

b) Quantification of Ki-67 positive cells in mice fed a control diet (CD-vehicle n=5, CD-DEN n=6) or high fat (HFD-vehicle n=6, HFD-DEN n=7) diet. Dashed line and p-value indicate a significant interaction effect between diet and DEN with two-way ANOVA testing.

c) Representative images of Ki-67 staining in livers of CD-vehicle HFD-vehicle CD-DEN and HFD-DEN, respectively. The red scale bar represents a length of 200 µm.

d) Quantification of F4/80 in liver sections from mice fed a control diet (CD-vehicle n=5, CD-DEN n=6) high-fat diet (HFD-vehicle n=6, HFD-DEN n=7) for 8-weeks. Quantification was conducted by measuring the total area with signal normalized to total cell count for the same image, with 3 random images per liver section analyzed.

e) Quantification of Ly6C/Ly6G in liver sections from mice fed a control diet (CD-vehicle n=5, CD-DEN n=4) high-fat diet (HFD-vehicle n=3, HFD-DEN n=4) for 8-weeks. Quantification was conducted by measuring the total area with signal normalized to total cell count for the same image, with 3 images per mouse.

f, g) Representative images of F4/80 and Ly6C/Ly6G staining in livers of CD-Vehicle, CD-DEN, HFD-Vehicle, and HFD-DEN. Scale bar represents 100µM (F4/80) or 100um (Ly6C/Ly6G), as noted on each image. Yellow arrows identify Ly6C/Ly6G stained cells.

Statistics: two-way ANOVA with Tukey's multiple comparison testing to test for differences between groups. Data are represented as median, with the boxes ranging from the 25th to the 75th percentile, whiskers go from minimum to maximum.

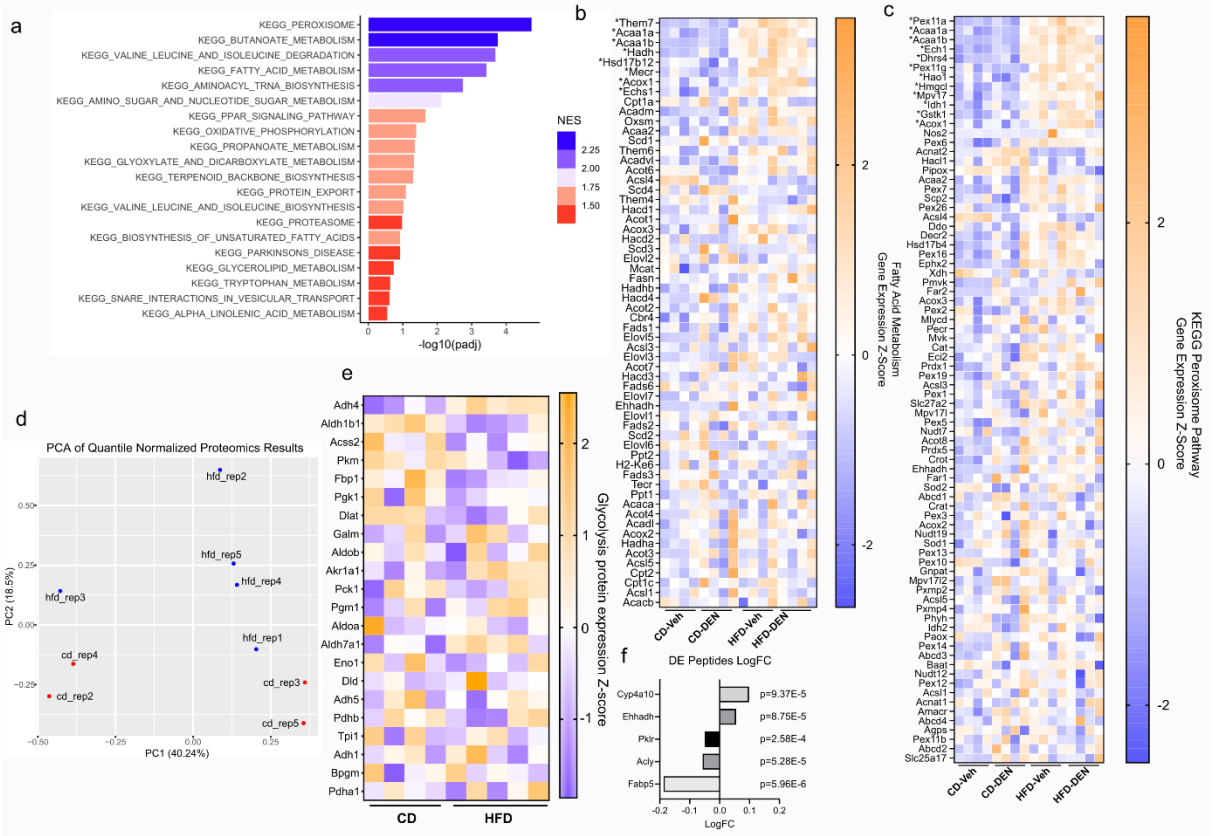

Figure S3: Transcriptomic and proteomic analysis of mouse livers exposed to 8-weeks of high-fat diet.

a) List of the top 20 upregulated KEGG pathways when comparing control diet (CD-vehicle and CD-DEN) to high-fat diet (HFD-vehicle and HFD-DEN). x-axis indicates the log(10) transformed adjusted p-value for each pathway listed, and the color scale indicates the normalized enrichment score (NES) calculated during gene set enrichment analysis (GSEA).

b) Heatmap of fatty acid metabolism gene expression in control diet (CD-vehicle, CD-DEN) and high fat diet (HFD-vehicle, and HFD-DEN) mouse livers expressed as Z-score (n=4 for all groups. * indicates genes that are significantly different with DESeq analysis testing for a diet effect, with p-adjusted < 0.05 considered significant.

c) Heatmap of genes in the KEGG Peroxisome pathway in control diet (CD-vehicle, CD-DEN) and high fat diet (HFD-vehicle, and HFD-DEN) mouse livers expressed as Z-score (n=4 for all groups). * indicates genes that are significantly different with DESeq analysis testing for a diet effect, with p-adjusted < 0.05 considered significant.

d) Principle coordinate analysis (PCA) for normalized proteomics data from control diet (n=4) and high fat diet (n=4) fed mice (no vehicle or DEN-injected mice included in this analysis). The proteomics data showed a high level of intra-group variation, despite relatively low amounts of missingness in the dataset (a potential source of variation). In the PCA representation of this data, the two sample groups were not well separated by the first two principle components (40.2% and 18.5% of the variance respectively) and consequently this may have hampered discovery of differentially enriched peptides (**Fig S3e,f**).

e) Heatmap showing z-score values for differential expression of proteins involved in glycolysis in control diet (n=4) and high fat diet (n=5) fed liver samples expressed as a Z-score.

f) Bar plot of the 5 differentially expressed (DE) peptides based on log fold-change (LogFC) identified in high fat diet fed mouse livers (n=5) compared to control diet livers (n=4) via Limma (Linear models for microarray data) differential expression analysis with p-values.

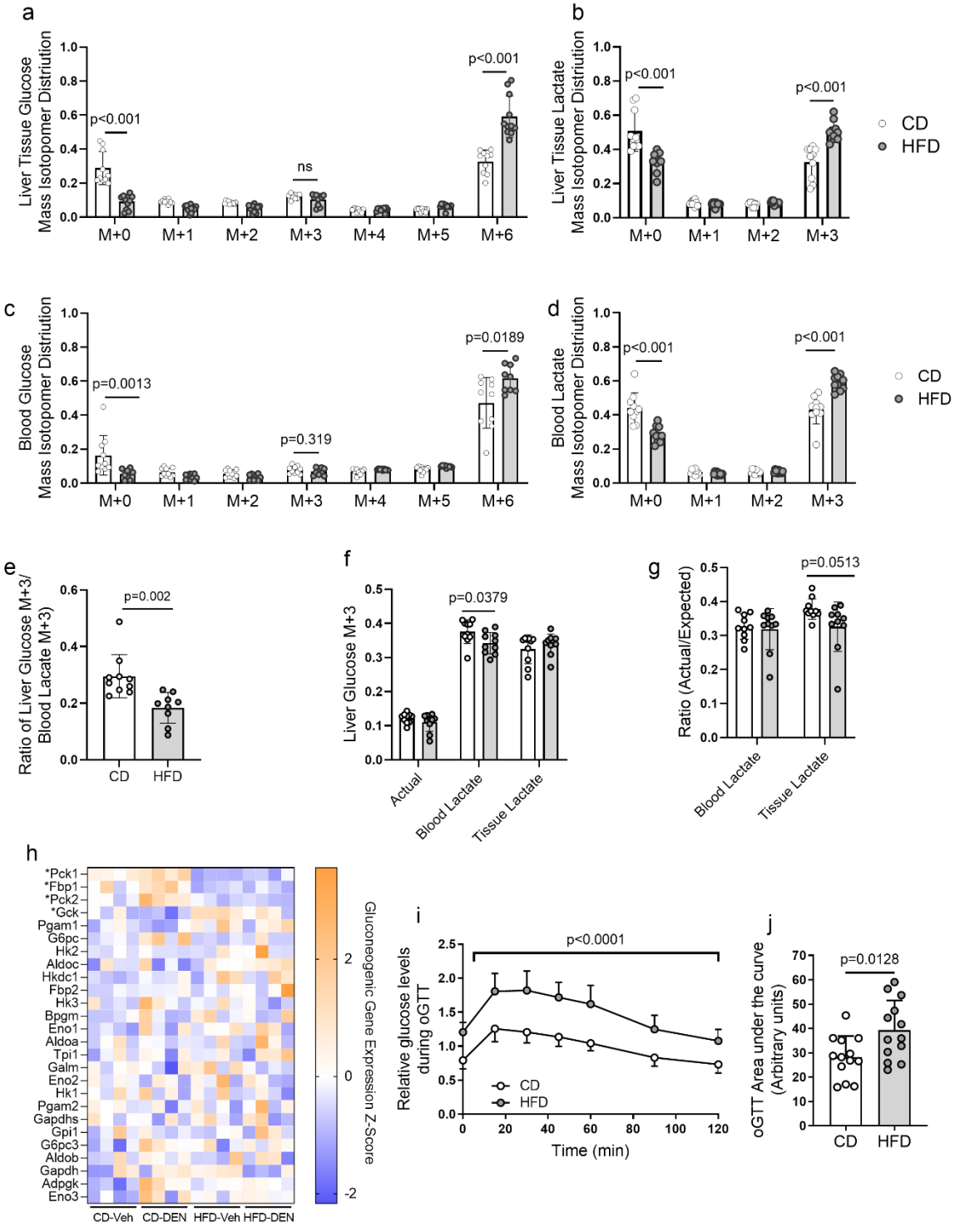

Figure S4: Labelling analysis for Cori cycle contributions and oral glucose tolerance of mice after 8-weeks on high fat or control diet.

Description of analysis of Cori Cycle contributions: The liver is part of the Cori cycle, *i.e.* glucose is converted by non-liver tissue to lactate, which is taken up by the liver to fuel glucose production via gluconeogenesis. To determine whether alterations in Cori cycle activity were contributing to the ^{13}C enrichment of hepatic lactate in HFD animals, we utilized the labelling data (a-d) and compared them to the theoretical contributions of blood lactate to liver glucose. We first determined the ratio of liver

glucose M+3 to blood lactate M+3, an indicator of altered Cori cycle activity, and found it was decreased in HFD compared to control (e). We then calculated the theoretical maximal contribution of blood lactate to liver glucose, which, in line with our measured data, was decreased in HFD mice (f). Comparing our observed values to theoretical maximal contributions we found that approximately 30% of liver glucose may originate from Cori cycle activity, and, importantly, was unaffected by HFD exposure (g). Accordingly, we found no HFD-induced changes in hepatic gene expression for the gluconeogenic enzymes glucose-6-phosphatase (*G6pc*) and a decreased expression of fructose-1,6-bisphosphatase (*Fbp1*) in our RNA-Seq dataset (h). Thus, we concluded that altered Cori cycle activity was not contributing to the ^{13}C enrichment of hepatic lactate in HFD fed mice.

a-b) Pooled MDV values for liver glucose and lactate from control diet (CD-vehicle n= 5, CD-DEN n=5) and high-fat diet fed mice (HFD-vehicle n=5, HFD-DEN n=5).

c-d) Pooled MDV values for blood glucose and lactate from control diet (CD-vehicle n= 5, CD-DEN n=5) and high-fat diet fed mice (HFD-vehicle n=5, HFD-DEN n=5).

e) Ratio of liver glucose M+3 to blood lactate M+3 in control diet (CD-vehicle n= 5, CD-DEN n=5) and high-fat diet fed mice (HFD-vehicle n=5, HFD-DEN n=5). Statistics: unpaired, two-tailed Student's t-test.

f) Comparison of actual liver glucose M+3 levels to expected liver glucose M+3 if all of it was being produced by lactate present in the liver tissue or blood. An explanation of this calculation is provided in the method section.

g) Ratio of observed liver glucose M+3 levels to the expected liver glucose M+3 levels represented in f). If this ratio approaches a value of 1, it would suggest that liver glucose is being produced via lactate in the liver tissue or blood.

h) Heatmap of gluconeogenic gene expression in control diet (CD-vehicle, CD-DEN) and high fat diet (HFD-vehicle, and HFD-DEN) mouse livers expressed as Z-score (n=4 for all groups). Some genes involved in gluconeogenesis overlap with glycolysis, and are repeated in **Fig. 1e**. * indicates genes that are significantly different with DESeq analysis testing for a diet effect, with p-adjusted < 0.05 considered significant.

i, j) Oral glucose tolerance test (oGTT, 2 g per kg body weight) performed on mice fed a control diet (CD-DEN; n=13) or high fat (HFD-den=13) for 8-weeks, and is represented by the change in blood glucose levels normalized across experiments and area under the curve. Statistics: two-way ANOVA with p-value for overall diet effect indicated (i) and unpaired, two-tailed Student's t-test (j).

Statistics: unless otherwise stated, unpaired two-tailed Student's t-testing, corrected for multiple testing with Holm-Sidak method if multiple testing was conducted (panels a-d), with $p<0.05$ considered significant. Data for all figures is average ± standard deviation.

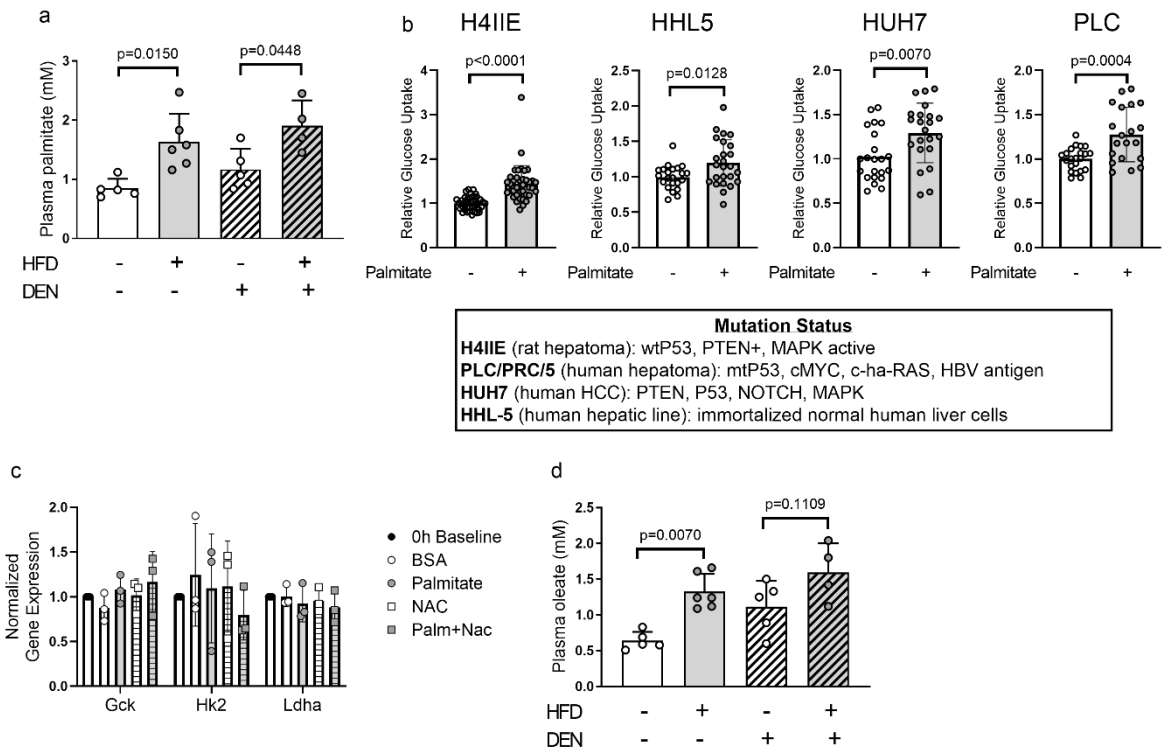

Figure S5: Blood plasma fatty acid concentrations are increased in mice after 8-weeks on high fat diet and oleate attenuates palmitate-stimulated glucose uptake.

a) Quantification of blood plasma palmitate concentrations (mM) in mice fed a control diet (CD-vehicle n=5, CD-DEN n=5) or high fat diet (HFD-vehicle n=6, HFD-DEN n=4) for a period of 8-weeks.

b) Glucose uptake in H4IIE, HHL5, HUH7, and PLC cell lines treated with 0.4 mM palmitate for 8-hours normalized to control. n=26-42 replicates. Text inset describes the mutational status of the different cell lines represented. Statistics: two-tailed unpaired Student's T-testing, with p-values as noted.

c) Gene expression of glucokinase (Gck), hexokinase 2 (HK2), and lactate dehydrogenase (Ldha) in H4IIE cells with 8-hours of 0.4mM palmitate treatment with or without 5mM NAC. Gene expression is normalized to untreated control cells collected at the 0-hour baseline.

d) Quantification of blood plasma oleate concentrations (mM) in mice fed a control diet (CD-vehicle n=5, CD-DEN n=5) or high fat diet (HFD-vehicle n=6, HFD-DEN n=4) for a period of 8-weeks.

Data for all figures is average ± standard deviation. Statistics: Unless noted otherwise, one-way ANOVA with Tukey's multiple comparison testing.

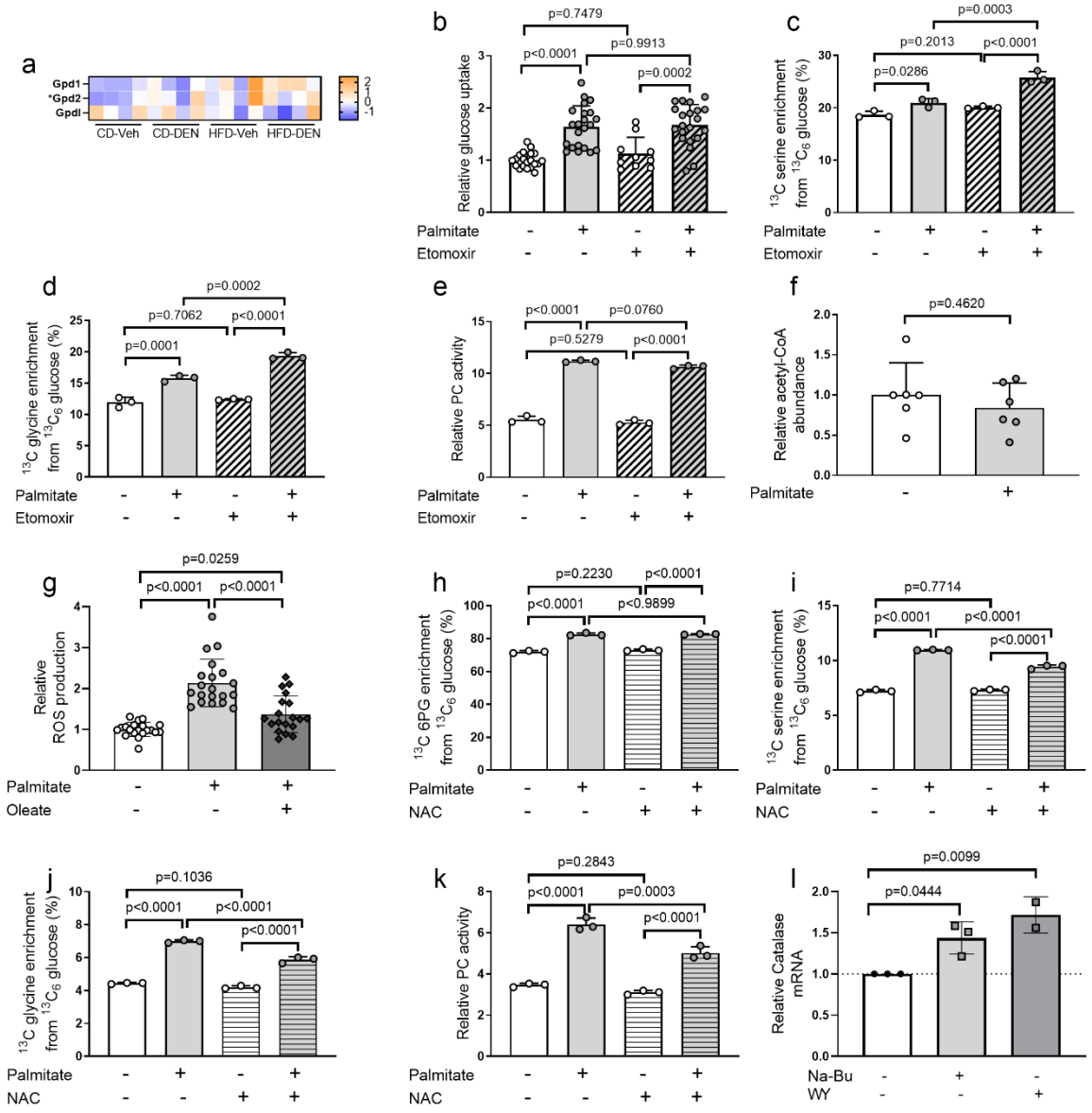

Figure S6: *Gpd* gene expression in mouse liver tissue after 8-weeks of high-fat diet and metabolic response of H4IIC3 cells to palmitate with or without etomoxir, oleate, and NAC.

a) Heat map with of *Gpd1*, *Gpd2*, and *Gpdl* in liver tissue from mice fed control diet (CD-vehicle n=4 and CD-DEN n=4) or high-fat diet (HFD-vehicle n=4 and HFD-DEN n=4) for 8-weeks, expressed as a Z-score. * indicates p-adjusted value <0.05 in DESeq testing for diet effect.

b-e) Glucose uptake (n=6 for each group, except etomoxir treatment n=5) (b), serine synthesis (n=3 for each group) with conversion to glycine (n=3 for each group) (c, d) and pyruvate carboxylase activity (n=3 for each group) (e) in H4IIC3 cells treated with 0.4 mM palmitate and/or 10 µM of etomoxir (CPT1α inhibitor) for a period of 8-hours normalized to control.

f) Acetyl-CoA abundance in cells treated with 0.4 mM palmitate for a period of 8-hours (n=6 for each group) normalized to control. Statistics: two-tailed unpaired Student's T-test.

g) ROS production in cells treated with 0.4 mM palmitate alone or in combination with 0.4mM oleate for 8-hours normalized to control (n=4 independent experiments with individual replicates plotted).

h-k) Synthesis of 6-phosphogluconate (6PG)(h), Serine biosynthesis (n=3 for each group)(i) with conversion to glycine (n=3 for each group)(j), and PC activity (n=3 for each group)(k) and in H4IIEC3 cells exposed for 8h to 0.4 mM palmitate or vehicle (ethanol) upon treatment with NAC (5 mM)
l) Catalase gene expression in H4IIE cells treated with 5mM of sodium butyrate (Na-Bu) or 100µM of WY-14643 (WY) for 24-hours. (n=2-3 independent experiments, normalized to vehicle control).
Data for all figures is average ± standard deviation. Statistics: Unless noted otherwise, One-way ANOVA with Tukey's multiple comparison testing.

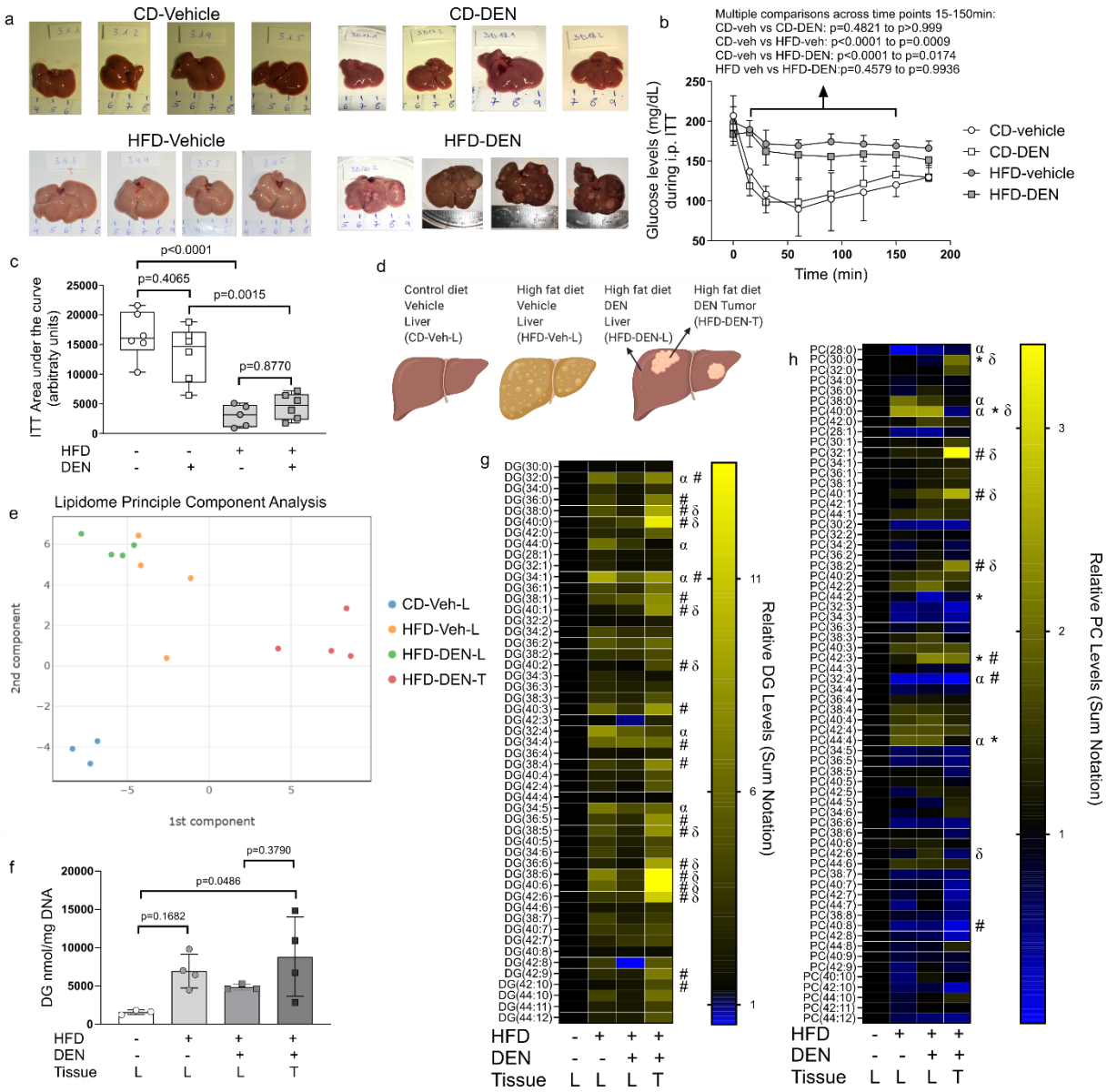

Figure S7: Tumor development and insulin tolerance upon carcinogen treatment and high fat diet feeding and alterations of the liver and tumor lipidome with high-fat diet and HCC tumor development.

a) Representative images of livers from mice fed a control diet or a high fat diet for a period of 29-weeks.

b,c) Intraperitoneal insulin tolerance test (i.p. ITT) in mice after 29-weeks on control diet (CD-vehicle n=6, CD-DEN n=6) or high fat diet (HFD-vehicle n=6, HFD-DEN n=6) with DEN or vehicle (Veh) treatment at the age of 2-weeks, expressed as blood glucose levels (mg/dL) and area under the curve. Statistics: Two- way ANOVA followed by Dunnett's multiple comparisons, with p-value ranges for the 15-150min time points included; during these time points significant differences were found between CD-vehicle and HFD-vehicle, and CD-vehicle and HFD-DEN, but not for CD-vehicle and CD-DEN, or HFD-vehicle and HFD-DEN. At the earlier and later time points, these significant differences diminished.

d) Schematic outlining the 4 groups used for lipidomics analysis: control diet vehicle liver (CD-Veh-L), high fat diet vehicle liver (HFD-Veh-L), and paired high fat diet DEN liver (HFD-DEN-L) and high fat diet DEN tumor tissue (HFD-DEN-T).

e) Principle component analysis for lipidomics analysis of control diet vehicle liver tissue (CD-Veh-L, n=3), high-fat diet vehicle liver tissue (HFD-Veh-L, n=4), high-fat diet DEN liver tissue (HFD-DEN-L, n=4) and adjacent high-fat diet DEN tumor tissue (HFD-DEN-T, n=4).

f) Total levels of diacylglycerides (DG) in control diet vehicle liver tissue (CD-Veh, n=3), high-fat diet vehicle liver tissue (HFD-Veh, n=4), high-fat diet DEN liver tissue (HFD-DEN-L, n=4) and adjacent high-fat diet DEN tumor tissue (HFD-DEN-T, n=4). L= liver tissue, T= tumor tissue in x-axis label. Statistics: one-way ANOVA with Tukey's multiple comparisons testing.

g) Heatmap of diacylglyceride (DG) sum notations, normalized to control diet vehicle liver tissue (CD-Veh, n=3), high-fat diet vehicle liver tissue (HFD-Veh, n=4), high-fat diet DEN liver tissue (HFD-DEN-L, n=4) and adjacent high-fat diet DEN tumor tissue (HFD-DEN-T, n=4). α indicates significant differences between CD-Veh-L and HFD-Veh-L, # indicates significant differences between CD-Veh-L and HFD-DEN-T, and δ indicates significant differences between HFD-DEN-L and HFD-DEN-T with two-way ANOVA and Tukey's multiple comparison testing. $p<0.05$ is considered significant.

h) Heatmap of phosphatidylcholine (PC) sum notations, normalized to control diet vehicle liver tissue (CD-Veh, n=4), high-fat diet vehicle liver tissue (HFD-Veh, n=4), high-fat diet DEN liver tissue (HFD-DEN-L, n=4) and adjacent high-fat diet DEN tumor tissue (HFD-DEN-T, n=4). α indicates significant differences between CD-Veh-L and HFD-Veh-L, *indicates significant differences between CD-Veh-L and HFD-DEN-L, # indicates significant differences between CD-Veh-L and HFD-DEN-T, and δ indicates significant differences between HFD-DEN-L and HFD-DEN-T with two-way ANOVA and Tukey's multiple comparison testing. $p<0.05$ is considered significant.

Box plots represented as median, with the boxes ranging from the 25th to the 75th percentile, whiskers go from minimum to maximum. Data for bar graphs is average ± standard deviation.

Supplementary Methods

Animal surgery and infusion protocols – extended details

At 13- and 34-weeks of age mice were implanted with a jugular vein catheter as previously described and infused with $^{13}C_6$-glucose after one week recovery time *(1)* . Briefly, mice were anesthetized with isoflurane and a catheter was inserted in the jugular vein, and connected to an antenna protruding from the dorsal part of the mice. The mice were then allowed to recover for approximately 1 week. In the morning, prior to infusion, mice were fasted for 6-hours after which they were infused, in the absence of food, for a period of 6-hours with a solution of 500 mg/ml $^{13}C_6$-glucose, at a rate of 30 mg/kg/min for the 14 week old mice and 7.5 mg/kg/min for the 35 week old mice *(1, 2)*. This difference in infusion rates was established to prevent any possible complications related to increased glucose intolerance and/or insulin resistance that can occur in mice fed a high fat diet for a prolonged period of time. At the end of the infusion protocol for both time points, mice were sacrificed by injecting approximately 50 µl of a 60 mg/ml Nembutal solution (Vetoquinol). Blood was then quickly collected from the mice via cardiac puncture, stored in heparin coated tubes at 4˚C and centrifuged to separate the plasma, and was immediately stored at -80˚C. Tissues were immediately excised, washed in ice-cold saline, placed into pre-labelled bags and frozen using a liquid nitrogen-cooled biosqueezer. The bags were then placed in liquid nitrogen until all collections were finished and finally stored at -80°C until further processing. Where necessary tumors were rapidly separated from normal tissue prior to freezing with tumor and normal tissue being stored separately.

Glucose isolation from tissue and serum samples

For tissue glucose measurements after extraction, dried tissue samples were dissolved in 50 µL hydroxylamine/pyridine (2%wt of hydroxyamine in pyridine) and incubated for 1-hour at 90˚C, then centrifuged at maximum speed. 100 µL of propionic anhydride was added and incubated for 30 min at 60˚C. Samples were centrifuged and dried overnight in a vacuum concentrator at 4˚C. Samples were dissolved in 100 µL ethyl acetate, vortexed, centrifuged for 2 min at 14,000 rpm, and transferred to GC/MS vials. For serum glucose, 90 µL of methanol was added to 10µL of serum and frozen at -80˚C for 2-hours. Samples were centrifuged for 10 min at maximum speed, and supernatants were transferred to GC/MS vials.

Gas chromatography-mass spectrometry analysis

Dried samples were placed in a vacuum concentrator at 4°C for 30 min to remove any residual water vapor. Samples were then incubated for 90 min at 37°C with 20 µL of a 20 mg/mL solution of methoxyamine in pyridine. Afterwards, 7.5 µL were transferred to a new tube and were further incubated with 15 µl of N-(tert-butyldi-methylsilyl)-N-methyltrifluoroacetamide, (with 1% tert-butyldimethyl-chlorosilane) for 60 min at 60°C. Metabolites were measured with a 7890A GC system (Agilent Technologies) combined with a 5975C Inert MS system (Agilent Technologies). One µL of sample was injected in splitless mode with an inlet temperature of 270°C onto a DB35MS column (Agilent Technologies). Helium was the carrier gas with a flow rate of 1 mL/min. For the measurement of polar metabolites, the GC oven was held at 100°C for 3 min and then ramped to 300°C with a gradient of 2.5°C/min. For the analysis of fatty acids, total fatty acid samples were esterified with 500 µL 2% sulphuric acid in methanol for 180 min at 60°C or overnight at 50°C and extracted by addition of 600 µL hexane and 100 µL saturated aqueous NaCl. Samples were centrifuged for 5 min and the hexane phase was separated and dried by vacuum centrifugation. Samples were resuspended in hexane, after

which the resulting fatty acid methyl esters were measured with a 7890A GC system (Agilent Technologies, CA, USA) combined with a 5975C or a 7000 inert MSD system (Agilent Technologies, CA, USA). One microliter of each sample was injected in a 3:1 split mode with an inlet temperature of 270°C onto a DB35MS column (Agilent Technologies, CA, USA). Helium was used as a carrier gas with a flowrate of 1 mL/min. The oven was held at 80 °C for 1 min and ramped with 5°C/min to 300°C. The MS system was operated under electron impact ionization at 70 eV and a mass range of 100-650 amu was scanned.

Liquid chromatography-mass spectrometry analysis

For the detection of metabolites by LC-MS, a Dionex UltiMate 3000 LC System (Thermo Scientific) with a thermal autosampler set at 4°C, coupled to a Q Exactive Orbitrap mass spectrometer (Thermo Scientific) was used. Samples were resuspended in 50 µL of water and a volume of 10 µl of sample was injected on a C18 column (Acquity UPLC HSS T3 1.8µm 2.1x100mm). The separation of metabolites was achieved at 40°C with a flow rate of 0.25 ml/min. A gradient was applied for 40 min (solvent A: 10mM Tributyl-Amine, 15mM acetic acid – solvent B: Methanol) to separate the targeted metabolites (0 min: 0% B, 2 min: 0% B, 7 min: 37% B, 14 min: 41% B, 26 min: 100% B, 30 min: 100% B, 31 min: 0% B; 40 min: 0% B. The MS operated in negative full scan mode (m/z range: 70-500 and 190-300 from 5 to 25 min) using a spray voltage of 4.9 kV, capillary temperature of 320°C, sheath gas at 50.0, auxiliary gas at 10.0. Data was collected using the Xcalibur software (Thermo Scientific).

For the detection of metabolites by LC-MS/MS, a 1290 Infinity II with a thermal autosampler set at 4°C, coupled to a 6470 triple quadrupole (Agilent Technologies) was used. Samples were resuspended in 60% acetonitrile and a volume of 4 µL of sample was injected on a SeQuant ZIC/pHILIC Polymeric column (Merck Millipore). The separation of metabolites was achieved at 25°C with a flow rate of 0.20 ml/min. A gradient was applied for 22 min (solvent A: 10mM ammonium acetate (pH=9.3, 10 mM) – solvent B: acetonitrile) to separate the targeted metabolites. (0 min: 10% A, 2 min: 10% A, 13 min: 30% A, 13.1 min: 70% A, 17 min: 75% A, 18 min: 10% A, 22 min: 10% A). The temperature of the gas and the sheath gas was set at 270°C (flow: 10L/min) and 300°C (flow: 12L/min), respectively.

PET imaging studies.

Mice were imaged using a Focus 220 small-animal PET system (Siemens Medical Solutions, Knoxville, TN, USA) using ^{18}F-FDG to image the glucose metabolism of the liver. Before injection with ^{18}F-FDG, the mice were restricted from food for at least 6-hours. Mice were anaesthetized with 2% isoflurane (Piramal Healthcare) in 100% O_2 (2 L/min) and 11 MBq of ^{18}F-FDG was administered by tail vein injection. Lasix was injected intramuscular to be able to empty the bladder of the mice just before scanning. Additionally, to simulate the effects of glucose infusions, mice were injected intraperitoneally with 600 µg/g of glucose (2.4µl/g of a 250 mg/ml solution). One hour after the injections, 10-minute static scans were performed. For every scan, a transmission scan was obtained using a ^{57}Co-source (Eckert & Ziegler, Berlin, Germany). PET images were reconstructed through a *maximum a posteriori* (MAP) reconstruction algorithm and further analyzed with PMOD 3.0 (PMOD technologies, Zürich, Switzerland). Images were converted to standardized uptake values (SUV), calculated according to the following formula: SUV is activity concentration in organ divided by injected activity per unit of weight of the animal. Volumes of interest (VOI) were positioned manually around the liver. The SUV values were then standardized to the total lean weight of the animals. Body

composition and bone mineral density of the total body with exclusion of the cranium was analyzed by dual-energy X-ray absorptiometry (DEXA; PIXImus densitometer; Lunar, Madison, WI, USA; software version 2.10.041)

Analysis of human glucose and lactate data

To determine if these patients showed any defects in glucose metabolism, we calculated the Matsuda index, the HOMA-IR, insulinogenic Index and Disposition index, using thresholds of ≤2.5, ≥2.5, ≤0.4 and ≥1 as cutoff for indicating defects in glucose metabolism (**Table S7**). Since all of the patients received a bolus of 75 g of glucose, regardless of weight, we decided to correct their determined blood lactate values by their estimated blood volume, using the equations 1 (for male patients) and equation 2 for female patients (Nadler's formula *(3)*).

$$blood\ volume = 0.3669h^3 + 0{,}03219w + 0.6041\ (eq.1)$$
$$blood\ volume = 0.3561h^3 + 0{,}03308w + 0.1833\ (eq.2)$$

Where *h* is the patient's height in meters and *w* is the patient's weight in kilograms. Subsequently, we multiplied the estimated blood volume by the total concentration of plasma lactate to obtain an estimation of the total amount of circulating lactate. This correction is necessary for analysis as, unlike in the mouse experiments, the dose of glucose given to patients is not standardized towards the weight of the patient and, therefore, a patient with higher blood volume will tend to have a smaller concentration of released lactate. The total amount of lactate was then plotted over time, and areas under the curve were determined using Graphpad Prism. Afterwards, the correlation between waist circumference and the total areas under the curve for the lactate kinetics or the maximal plasma lactate values was calculated using Graphpad Prism, using an F-test to determine deviation from 0-slope. Maximal lactate values were calculated between 10 min and 150 min post glucose ingestion, to prevent confounding effects from two patients, whose lactate maximal values were at time -10 min (before glucose ingestion) and time 240 min.

Preparation of solutions for cell culture experiments

Sodium palmitate (Sigma-Aldrich) was dissolved in a 50% ethanol solution to a concentration of 195 mM, this solution was made homogeneous by warming it to approximately 45°C. The palmitate solution was then quickly added to a pre-warmed 10% Bovine serum albumin (BSA) (Sigma-Aldrich) solution (dissolved in DMEM) to a final concentration of 3mM. The BSA-Palmitate mix was then incubated at 37°C with occasional gentle mixing for 1-hour to promote the formation of BSA-palmitate complexes. This solution can be stored at -20°C until further use. 3mM BSA-palmitate solutions were then finally diluted in DMEM to achieve a final concentration of 0.4 mM in the cultured cells. Control solutions were prepared the same way, using a pure 50% ethanol solution. Following this protocol, the final concentration of ethanol in the cells is approximately 0.1%. Etomoxir was dissolved in distilled water at a concentration of 50 mM and used at a final concentration of 10 µM. N-acetyl-L-Cysteine (NAC) was dissolved in DMEM media at a concentration of 25 mM. The pH was then adjusted to 7.3, and the solution further diluted in DMEM for final concentration of 5 mM. Mitotempo was dissolved in water to a concentration of 10 mM. ATZ was dissolved in water at a concentration of 2M. Sodium butyrate (Na-Bu) was dissolved in DMEM media at a stock concentration of 50mM and diluted to 5mM. WY-14643 was diluted in 100% ethanol at a stock concentration of 50mM and diluted to 100µM.

Whenever ^{13}C tracers were used all the aforementioned solutions were dissolved in DMEM where regular glucose was replaced with $^{13}C_6$-glucose to prevent any possible dilutions of the tracer.

Calculation for lactate secretion from H4IIE cells labelled with $^{13}C_6$-glucose.

Lactate secretion was calculated with the assumption of exponential growth, using the following equation, where Gi indicates the rate of nutrient secretion, Ci(0) is the initial lactate concentration at time = 0-hours, Ci (Δt) is the lactate concentration at t = 8-hours for the present experiments, N(0) is the number of cells at t = 0h, N(Δt) is the number of cells at the final time point of 8-hours. Lactate secretion was normalized to control conditions, and expressed as a fraction of control.

$$Gi = \frac{Ci(0) - Ci(\Delta t)}{\Delta t(N(0) - N(\Delta t))} \cdot ln\left[\frac{N(0)}{N(t)}\right]$$

Quantitative real-time PCR process details

The relative levels of gene transcripts compared to the control gene Ppib (cyclophilin B, FW 5'-CAAAATTGGAGACGAACCTG-3', RV: 5'- GAAGTCTCCACCCTGGATCA-3') and catalase (Cat1, FW: 5'-TGACCTCAGAAACGACAACG-3', RV: 5'-TTGTCCAGAAGAGCCTGGAT-3' were determined by quantitative real-time PCR using SYBER GreenPCR Master Mix (Life Technologies) and specific primers on a 7500 Fast Real Time PCR System (Applied Biosystems, Life Technologies). Amplification was performed at 95°C for 10 min, followed by 40 cycles of 15 s at 95°C and 1 min at 60°C. In order to quantify differences between groups, we calculated expression fold change by using the equation:

$$fold\ change = 2^{-\Delta\Delta Ct}\ (eq.3)$$

***In silico* metabolic comparison of proliferating cells and palmitate-treated cells.**

In order to determine if there is any potential metabolic overlap between cells exposed to palmitate (as a simulation of a high fat diet) *versus* highly proliferative cells (as a simulation of hepatic cancer cells), we applied an algorithm termed *differential flux-balance analysis* (DFA) to the genome-scale metabolic network model HepatoNet1 *(4)*. Briefly, this model includes 785 metabolites and 2,589 reactions across 8 cellular compartments, resulting in a total of 1445 compartment-specific metabolites. Flux balance analysis (FBA) is a standard mathematical procedure to semi-quantitatively estimate the metabolic flux of each reaction in a genome-scale model at steady state when satisfying a given metabolic objective (*objective function optimization*), such as the production or consumption of given metabolites. In our DFA implementation, we analyze the average change in metabolic fluxes when optimizing each of 442 metabolic objective functions included in Hepatonet1 in standard physiological conditions versus perturbed non-physiological conditions. Non-physiological conditions are simulated by imposing additional constraints on metabolic reactions, metabolic objectives, or both. Finally, the change in metabolic fluxes between the standard and perturbed model are computed to yield differential fluxes. Then, the differential fluxes involving the same metabolite are aggregated in order to rank metabolites. In the resulting ranked list, metabolites on top will be the ones involved in the metabolic fluxes that change the most. In this study, we defined two altered models: *palmitate utilization* and *cell growth*. Palmitate utilization was simulated by imposing palmitate reduction in the cytosol as an additional term (*-palmitate(c)*) in all the 442 metabolic objective functions. Analogously, for the cell growth model we added the production of all amino acids and nucleotides as additional

terms to each objective function (*+ Alanine(c) + Arginine(c) … + dATP(c) + dCTP(c)...*). For each of the two models, we simulated the realization of all the 442 altered objective functions and compared (absolute difference) the resulting fluxes to those obtained with the same method applied to the physiological model. We finally averaged such differential fluxes values over all the objective functions, and from these we ranked the metabolites to obtain the final estimates. More details on the method can be found in our previous publication *(4)*.

Analysis of gas chromatography-gas spectrometry data

Mass distribution vectors were extracted from the raw ion chromatograms using a custom Matlab script *(5, 6)* (available upon reasonable request), which applies consistent integration bounds and baseline correction to each ion. Moreover, we corrected for naturally occurring isotopes using the method of Fernandez et al *(7)*. Fractional contribution (FC) of the glucose tracer to each molecule of interest was calculated using the following equation:

$$FC = \frac{\sum_{i=0}^{n} i \cdot m_i}{n \cdot \sum_{i=0}^{n} i \cdot m_i} (eq. 4)$$

Where *n* is the number of carbon atoms in the metabolite, *i* the different isotopomer abundances and *m* the abundance for each mass. The abundance of metabolites was also standardized towards the respective internal standard, i.e., glutarate for organic acids and norvaline for amino acids.

For *in vivo* experiments, the fractional contribution (FC) of each metabolite was normalized towards the FC of plasma glucose, according to the equation below and as described previously *(2, 8, 9)*:

$$normalized\ FC_x = \frac{FC_x}{FC_{plasma\ glucose}}$$

Where x represents any given metabolite. This equation corrects for any potential differences of the actual tracer enrichment ($^{13}C_6$ glucose) between mice.

Pyruvate carboxylase (PC) activity was determined in $^{13}C_6$ glucose tracer experiments as previously described, using the following equation *(10, 11)*:

$$PC\ acitivity = malate\ (M+3) - succinate\ (M+3)\ (eq, 6)$$

Briefly, the glucose-generated M+3 enrichment in malate can originate from both PC activity or oxidative TCA cycle activity, whereas glucose derived succinate M+3 labelling, can only be generated via the TCA cycle, assuming a low to nonexistent reverse flux through succinate dehydrogenase. Additionally, metabolite values were standardized towards sample weight (in case of tissues), extracted volume (for plasma extractions) or cell number (for *in vitro* studies).

Exploration of the involvement of the Cori cycle, and contribution of circulating or tissue lactate to glucose production was calculated using observed MDVs for glucose and lactate measured in liver tissue and blood samples. Considering 2 lactate molecules are required to produce 1 glucose molecule, we used the following calculation to estimate maximal abundance of glucose M+3 if all glucose production was coming from available lactate:

$$\text{Liver Glucose}_{M+3} = 2 \times \text{Lactate}_{M+0} \times \text{Lactate}_{M+3} + 2 \times \text{Lactate}_{M+1} \times \text{Lactate}_{M+2}$$

This value was then used to compare to actual observed levels of glucose M+3 to draw conclusions on the relative contribution of the Cori cycle to liver glucose levels.

Analysis of liquid chromatography-gas spectrometry data

The data were analyzed with Matlab for the correction of protein content and natural abundance, but also to determine the isotopomer distribution using the method developed by Fernandez *et al*., 1996 *(7)*.

RNA Sequencing and Transcriptomics Analysis

RNA from liver tissues were extracted using TRiazol (Life Technologies), with chloroform and propanol for phase separation and RNA isolation. RNA quality and quantity were measured using a NanoDrop One Microvolume UV-Vis Spectrophotometer (Thermo Scientific). Total RNA from control diet vehicle, control diet DEN, high fat diet vehicle, and high-fat diet DEN liver tissue from mice exposed to high fat diet for 8-weeks (n=4 per group) were sequenced. RNAseq libraries were prepared from 1 µg of total RNA per sample using the KAPA Stranded mRNA Sequencing Kit (Roche). In short, poly-A containing mRNA was purified from total RNA using oligo(dT) magnetic beads and fragmented into 200–500 bp pieces using divalent cations at 94ºC for 8 min. The cleaved RNA fragments were copied into first strand cDNA. After second strand cDNA synthesis, fragments were A-tailed and indexed adapters were ligated. The products were purified and enriched by PCR to create the final cDNA library. After quantification with qPCR, the resulting libraries were sequenced on a HiSeq4000 (Illumina) using a flow cell generating 1x50bp single-end reads.

RNA data processing was conducted using an NGS pipeline to process the raw RNAseq reads and generate the count data used in the following RNAseq differential expression analysis. This pipeline was constructed using Snakemake (version 5.5.3) *(12)*, utilizing Bioconda software versioning system (version 4.8.2) *(13)*, Python (version 3.7.3), R (version 3.6.3 -- "Holding the Windsock") and ran on a HPC using Ubuntu Linux operating system (16.04.4 LTS x86_64). The raw fastq data was processed in the pipeline using the listed bioinformatics tools in the following steps:

A first round of quality control was performed with FastQC (version 0.11.8) FastQC on each raw R1 fastq.gz file and the read quality, sequence quality per position, overall sequence quality and duplication levels were inspected. The processed files were trimmed of the universal adapter by Trimmomatic (version 0.36) *(14)*. A second round of QC was performed via FastQC on the trimmed files. The Phred score was determined to be >30 across all bases and other criteria were found to be within acceptable limits. The trimmed fastq.gz files were aligned using hisat2 (version 2.1.0) *(15)* on the GRCm38_snp_tran Genome Reference Consortium Mouse Build 38 reference assembly *(16)*. The resulting .bam files were sorted and indexed using samtools (version 1.9) *(17)*. For each sample, indexed files were used to generate count files using htseq-count (version 0.11.1) *(18)* with the Mus_musculus.GRCm38.102.gtf.gz as reference. The count files for each sample were collated into a single count matrix .csv file.

The RNAseq count data was analyzed using the Bioconductor package, DESeq2 (version 1.30.0) *(19)*. The counts were modeled using the following designs: control vs DEN, control vs HFD and an interaction model ~ DEN * HFD, setting CD_PBS as the intercept. Genes with row counts of all 0 for all samples were removed before DESeq2 analysis. Three different comparisons were performed for the following groups with an FDR cutoff = 0.05: 1) control vs DEN 2) control vs HFD and 3) ~ DEN * HFD. Exploratory data analysis and quality control was performed, including PCA, comparison of sample-wise size factors, assessment of independent filtering thresholds and rejections versus the filter quantiles. MA plots and Volcano plots were created to visualize the differential expression.

The threshold of significance was set at p-adjusted value < 0.05, which was used to produce a list of enriched genes. Gene Ontology (GO) pathway enrichment analyses were performed utilizing limma::goana() (version 3.42.0) *(20)* with FDR cutoff = 0.05 on the list of enriched genes compared to a universe of all genes within the data that could be mapped to an ENTREZ ID using org.Mm.eg.db mouse genome annotation database (version 3.10.0) org.Mm.eg.db. Gene sets for GO terms and KEGG pathways were loaded from the Molecular Signatures Database (MsigDB) using hypeR::msigdb_gsets()from the hypeR R package *(21)*. The list of genes derived from the DESeq2 results were sorted by t-statistic, and tested against the GO and KEGG gene sets using fgsea::Multilevel() from the FGSEA package, with gene set minimum size = 1 and permutations = 1000 *(22)*. Select results of the GSE analyses were visualized using ggplot2 and Pathview *(23)*.

Proteomics and Analysis

Peptides were isolated from liver samples from control diet and high fat diet livers after 8-weeks of feeding (no vehicle or DEN-injected samples were used in this analysis due to potential interactions with $^{13}C_6$-glucose tracing) using the iST sample preparation kit (PreOmics, Germany). Purified peptides were re-dissolved in 20 µl loading solvent A (0.1% TFA in water/ACN (98:2, v/v)) and the peptide concentration was determined on a Lunatic instrument (Unchained Lab). 2µg peptides were injected for LC-MS/MS analysis on an Ultimate 3000 RSLCnano system in-line connected to a Q Exactive HF BioPharma mass spectrometer (Thermo). Trapping was performed at 10 µl/min for 4 min in loading solvent A on a 20 mm trapping column (made in-house, 100 µm internal diameter (I.D.), 5 µm beads, C18 Reprosil-HD, Dr. Maisch, Germany). The peptides were separated on a 250 mm Waters nanoEase M/Z HSS T3 Column, 100Å, 1.8 µm, 75 µm inner diameter (Waters Corporation) kept at a constant temperature of 50°C. Peptides were eluted by a non-linear gradient reaching 9% MS solvent B (0.1% FA in water/acetonitrile (2:8, v/v)) in 15 min, (33% MS solvent B in 90 min and 55% MS solvent B in 100 min and 97% MS solvent B in 125 min at a constant flow rate of 300 nl/min, followed by a 45-minute wash at 97% MS solvent B and re-equilibration with MS solvent A (0.1% FA in water). The mass spectrometer was operated in data-dependent mode, automatically switching between MS and MS/MS acquisition for the 16 most abundant ion peaks per MS spectrum. Full-scan MS spectra (375-1500 m/z) were acquired at a resolution of 60,000 in the Orbitrap analyzer after accumulation to a target value of 3,000,000. The 16 most intense ions above a threshold value of 13,000 were isolated with a width of 1.5 m/z for fragmentation at a normalized collision energy of 28% after filling the trap at a target value of 100,000 for maximum 80 ms. MS/MS spectra (200-2000 m/z) were acquired at a resolution of 15,000 in the Orbitrap analyzer.

LC-MS/MS runs of all 10 samples were searched together using the MaxQuant algorithm (version 1.6.11.0) with mainly default search settings, including a false discovery rate set at 1% on PSM, peptide

and protein level. Spectra were searched against the mouse protein sequences in the Swiss-Prot database (database release version of 2020_06), containing 17,042 sequences (www.uniprot.org) . Proteomic analysis was conducted with the raw peptide counts derived from MaxQuant results were analyzed for missingness and transformed to log counts and then quantile normalized. The normalized counts were transformed into an eSet using Msnbase *(24)*, and analyzed using limma using model CD vs HFD *(25)*. Volcano plots were created to visualize the differential peptide abundances.

Lipidomics and Analysis

Lipids were extracted from liver tissues by mixing 700 µL in water, homogenizing (Preellys, Bertin) with 800 µL 1 N HCl:CH3OH 1:8 (v/v), 900 µL $CHCl_3$, 200 µg/ml of the antioxidant 2,6-di-tert-butyl-4-methylphenol (BHT; Sigma Aldrich) and 3 µL of SPLASH® LIPIDOMIX® Mass Spec Standard (#330707, Avanti Polar Lipids). After vortexing and centrifugation, the lower organic fraction was collected and evaporated using a Savant Speedvac spd111v (Thermo Fisher Scientific) at room temperature and the remaining lipid pellet was stored at - 20°C under argon. Just before mass spectrometry analysis, lipid pellets were reconstituted in 100% ethanol. Lipid species were analyzed by liquid chromatography electrospray ionization tandem mass spectrometry (LC-ESI/MS/MS) on a Nexera X2 UHPLC system (Shimadzu) coupled with hybrid triple quadrupole/linear ion trap mass spectrometer (6500+ QTRAP system; AB SCIEX). Chromatographic separation was performed on a XBridge amide column (150 mm × 4.6 mm, 3.5 µm; Waters) maintained at 35°C using mobile phase A [1 mM ammonium acetate in water-acetonitrile 5:95 (v/v)] and mobile phase B [1 mM ammonium acetate in water-acetonitrile 50:50 (v/v)] in the following gradient: (0-6 min: 0% B → 6% B; 6-10 min: 6% B → 25% B; 10-11 min: 25% B → 98% B; 11-13 min: 98% B → 100% B; 13-19 min: 100% B; 19-24 min: 0% B) at a flow rate of 0.7 mL/min which was increased to 1.5 mL/min from 13 minutes onwards. SM, CE, CER, DCER, HCER, LCER were measured in positive ion mode with a precursor scan of 184.1, 369.4, 264.4, 266.4, 264.4 and 264.4 respectively. TAG, DAG and MAG were measured in positive ion mode with a neutral loss scan for one of the fatty acyl moieties. PC, LPC, PE, LPE, PG, PI and PS were measured in negative ion mode by fatty acyl fragment ions. Lipid quantification was performed by scheduled multiple reactions monitoring (MRM), the transitions being based on the neutral losses or the typical product ions as described above. The instrument parameters were as follows: Curtain Gas = 35 psi; Collision Gas = 8 a.u. (medium); IonSpray Voltage = 5500 V and −4,500 V; Temperature = 550°C; Ion Source Gas 1 = 50 psi; Ion Source Gas 2 = 60 psi; Declustering Potential = 60 V and −80 V; Entrance Potential = 10 V and −10 V; Collision Cell Exit Potential = 15 V and −15 V.

The following fatty acyl moieties were taken into account for the lipidomic analysis: 14:0, 14:1, 16:0, 16:1, 16:2, 18:0, 18:1, 18:2, 18:3, 20:0, 20:1, 20:2, 20:3, 20:4, 20:5, 22:0, 22:1, 22:2, 22:4, 22:5 and 22:6 except for TGs which considered: 16:0, 16:1, 18:0, 18:1, 18:2, 18:3, 20:3, 20:4, 20:5, 22:2, 22:3, 22:4, 22:5, 22:6. Peak integration was performed with the MultiQuant™ software version 3.0.3. Lipid species signals were corrected for isotopic contributions (calculated with Python Molmass 2019.1.1) and were quantified based on internal standard signals and adheres to the guidelines of the Lipidomics Standards Initiative (LSI) (level 2 type quantification as defined by the LSI). Unpaired T-test p-values and FDR corrected p-values (using the Benjamini/Hochberg procedure) were calculated in Python StatsModels version 0.10.1.

Radioactive measurement of glycolytic flux

Glycolytic rates were determined as previously described *(26)*. Briefly, cells were incubated for 8-hours in medium containing 1µCi/ml D-[5-^{3}H(N)]-glucose (Perkin Elmer). During glycolysis, triose phosphate isomerase releases the ^{3}H proton as a water molecule and, thus, measurement of radioactive activity of water can be used as a surrogate of glycolytic flux. To that end, after the 8-hour experiment, the growth media was transferred to glass vials and 100 µl of 12% perchloric acid was added, to prevent any metabolic activity of unintentionally transferred cells. A hanging well, containing a Whatman filter paper soaked with H_2O was then added to the vials after which they were capped using rubber stoppers and warmed at 37°C for a period of 48-hours. The evaporated ^{3}H containing water is captured by the filter and radioactivity can be measured directly using a scintillation counter (Perkin Elmer Tri-Carb 2810TR).

Histology and immunohistochemistry (IHC)

Tissue samples were fixed in 4% paraformaldehyde for 24-hours and processed for paraffin embedding (HistoStar™ Embedding Workstation). 4 µm thick sections were stained with hematoxylin and eosin (H&E). Antigen retrieval (ProTaqs IV Antigen Enhancer (401602392, Quartett)) and Ki-67 staining (VENTANA BenchMark system (Roche)) was conducted with an ultraView detection kit (Roche) and a monoclonal mouse anti-Ki-67 antibody (M7240, Agilent) with hematoxylin (H 3401, Vector Laboratories) counterstain. 10 high-power fields (×40 magnification) for each tumor sample were used for Ki67 analysis. F4/80 (mouse, 1:300, Serotec, MCA497) and Ly6C and Ly6G (Rat, 1:1000, BD Biosciences #553123) staining was conducted by immunoflourescence with tyramide signal amplification (PerkinElmer Opal 4-Color Manual IHC Kit, PerkinElmer/Akoya). Secondary antibody detection for rat Ly76C/Ly6G (ImmPRESS HRP Anti-Rat IgG (Peroxidase) Polymer Detection Kit, Vector Laboratories), and mouse F4/80 (OPAL Polymer HRP Ms+Rb, Akoya/Perkin Elmer) was conducted. Images were acquired on the Zeiss Axio Scan.Z1 using a x20 objective and ZEN 2 software. Analysis of F4/80 and Ly6C/Ly6G was conducted on 3 random selections per liver section at high-powered field, using FIJI (Image J 1.53c, NIH) by measuring total stained areas and normalizing to cell count (DAPI).

Supplemental Methods References

1. D. Broekaert, S. M. Fendt, Measuring in vivo tissue metabolism using 13C glucose infusions in mice, *Methods Mol. Biol.* **1862**, (Metabolic Signaling) (2019).

2. S. M. Davidson, T. Papagiannakopoulos, B. A. Olenchock, J. E. Heyman, M. A. Keibler, A. Luengo, M. R. Bauer, A. K. Jha, J. P. O'Brien, K. A. Pierce, D. Y. Gui, L. B. Sullivan, T. M. Wasylenko, L. Subbaraj, C. R. Chin, G. Stephanopolous, B. T. Mott, T. Jacks, C. B. Clish, M. G. Van Der Heiden, Environment impacts the metabolic dependencies of ras-driven non-small cell lung cancer, *Cell Metab.* **23**, 517–528 (2016).

3. S. B. Nadler, J. U. Hidalgo, T. Bloch, Prediction of blood volume in normal human adults, *Surgery* **51**, 224–32 (1962).

4. R. Pagliarini, R. Castello, F. Napolitano, R. Borzone, P. Annunziata, G. Mandrile, M. De Marchi, N. Brunetti-Pierri, D. di Bernardo, In Silico Modeling of Liver Metabolism in a Human Disease Reveals a Key Enzyme for Histidine and Histamine Homeostasis, *Cell Rep.* **15**, 2292–2300 (2016).

5. M. R. Antoniewicz, J. K. Kelleher, G. Stephanopoulos, Elementary metabolite units (EMU): A novel framework for modeling isotopic distributions, *Metab. Eng.* **9**, 68–86 (2007).

6. J. D. Young, J. L. Walther, M. R. Antoniewicz, H. Yoo, G. Stephanopoulos, An elementary metabolite

unit (EMU) based method of isotopically nonstationary flux analysis, *Biotechnol. Bioeng.* **99**, 686–99 (2008).

7. C. A. Fernandez, C. Des Rosiers, S. F. Previs, F. David, H. Brunengraber, Correction of 13C mass isotopomer distributions for natural stable isotope abundance, *J. Mass Spectrom.* **31**, 255–62 (1996).

8. K. D. Courtney, D. Bezwada, T. Mashimo, K. Pichumani, V. Vemireddy, A. M. Funk, J. Wimberly, S. S. McNeil, P. Kapur, Y. Lotan, V. Margulis, J. A. Cadeddu, I. Pedrosa, R. J. DeBerardinis, C. R. Malloy, R. M. Bachoo, E. A. Maher, Isotope Tracing of Human Clear Cell Renal Cell Carcinomas Demonstrates Suppressed Glucose Oxidation In Vivo, *Cell Metab.* **28**, 793-800.e2 (2018).

9. A. Quaegebeur, I. Segura, R. Schmieder, D. Verdegem, I. Decimo, F. Bifari, T. Dresselaers, G. Eelen, D. Ghosh, S. M. Davidson, S. Schoors, D. Broekaert, B. Cruys, K. Govaerts, C. De Legher, A. Bouché, L. Schoonjans, M. S. Ramer, G. Hung, G. Bossaert, D. W. Cleveland, U. Himmelreich, T. Voets, R. Lemmens, C. F. Bennett, W. Robberecht, K. De Bock, M. Dewerchin, B. Ghesquière, S. M. Fendt, P. Carmeliet, Deletion or inhibition of the oxygen sensor PHD1 protects against ischemic stroke via reprogramming of neuronal metabolism, *Cell Metab.* **23**, 280–91 (2016).

10. S. Christen, D. Lorendeau, R. Schmieder, D. Broekaert, K. Metzger, K. Veys, I. Elia, J. M. Buescher, M. F. Orth, S. M. Davidson, T. G. P. Grünewald, K. De Bock, S. M. Fendt, Breast Cancer-Derived Lung Metastases Show Increased Pyruvate Carboxylase-Dependent Anaplerosis, *Cell Rep.* **17**, 837–48 (2016).

11. J. M. Buescher, M. R. Antoniewicz, L. G. Boros, S. C. Burgess, A roadmap for interpreting 13C metabolite labeling patterns from cells, *Curr. Opin. Biotechnol.* **34**, 189–201 (2015).

12. J. Köster, S. Rahmann, Snakemake—a scalable bioinformatics workflow engine, *Bioinformatics* **34**, 3600 (2018).

13. R. Dale, B. Grüning, A. Sjödin, J. Rowe, B. A. Chapman, C. H. Tomkins-Tinch, R. Valieris, B. Batut, A. Caprez, T. Cokelaer, D. Yusuf, K. A. Beauchamp, K. Brinda, T. Wollmann, G. Le Corguillé, D. Ryan, A. Bretaudeau, Y. Hoogstrate, B. S. Pedersen, S. van Heeringen, M. Raden, S. Luna-Valero, N. Soranzo, M. De Smet, G. Von Kuster, R. Kirchner, L. Pantano, Z. Charlop-Powers, K. Thornton, M. Martin, M. van den Beek, D. Maticzka, M. Miladi, S. Will, K. Gravouil, P. Unneberg, C. Brueffer, C. Blank, V. C. Piro, J. Wolff, T. Antao, S. Gladman, I. Shlyakhter, M. de Hollander, P. Mabon, W. Shen, J. Boekel, M. Holtgrewe, D. Bouvier, J. R. de Ruiter, J. Cabral, S. Choudhary, N. Harding, R. Kleinkauf, E. Enns, F. Eggenhofer, J. Brown, P. J. A. Cock, H. Timm, C. Thomas, X. O. Zhang, M. Chambers, N. Turaga, E. Seiler, C. Brislawn, E. Pruesse, J. Fallmann, J. Kelleher, H. Nguyen, L. Parsons, Z. Fang, E. B. Stovner, N. Stoler, S. Ye, I. Wohlers, R. Farouni, M. Freeberg, J. E. Johnson, M. Bargull, P. R. Kensche, T. H. Webster, J. M. Eppley, C. Stahl, A. S. Rose, A. Reynolds, L. B. Wang, X. Garnier, S. Dirmeier, M. Knudsen, J. Taylor, A. Srivastava, V. Rai, R. Agren, A. Junge, R. V. Guimera, A. Khan, S. Schmeier, G. He, L. Pinello, E. Hägglund, A. S. Mikheyev, J. Preussner, N. R. Waters, W. Li, J. Capellades, A. T. Chande, Y. Pirola, S. Hiltemann, M. L. Bendall, S. Singh, W. A. Dunn, A. Drouin, T. Di Domenico, I. de Bruijn, D. E. Larson, D. Chicco, E. Grassi, G. Gonnella, J. B, L. Wang, F. Giacomoni, E. Clarke, D. Blankenberg, C. Tran, R. Patro, S. Laurent, M. Gopez, B. Sennblad, J. A. Baaijens, P. Ewels, P. R. Wright, O. M. Enache, P. Roger, W. Dampier, D. Koppstein, U. K. Devisetty, T. Rausch, M. Cornwell, A. E. Salatino, J. Seiler, M. Jung, E. Kornobis, F. Cumbo, B. K. Stöcker, O. Moskalenko, D. R. Bogema, M. L. Workentine, S. J. Newhouse, F. da V. Leprevost, K. Arvai, J. Köster, Bioconda: Sustainable and comprehensive software distribution for the

life sciences, *Nat. Methods* **15**, 475–6 (2018).

14. A. M. Bolger, M. Lohse, B. Usadel, Trimmomatic: A flexible trimmer for Illumina sequence data, *Bioinformatics* **30**, 2114–20 (2014).

15. D. Kim, J. M. Paggi, C. Park, C. Bennett, S. L. Salzberg, Graph-based genome alignment and genotyping with HISAT2 and HISAT-genotype, *Nat. Biotechnol.* **37**, 097–15 (2019).

16. Y. Q. S. Soh, J. Alföldi, T. Pyntikova, L. G. Brown, T. Graves, P. J. Minx, R. S. Fulton, C. Kremitzki, N. Koutseva, J. L. Mueller, S. Rozen, J. F. Hughes, E. Owens, J. E. Womack, W. J. Murphy, Q. Cao, P. De Jong, W. C. Warren, R. K. Wilson, H. Skaletsky, D. C. Page, Sequencing the mouse y chromosome reveals convergent gene acquisition and amplification on both sex chromosomes, *Cell* **159**, 800–13 (2014).

17. H. Li, B. Handsaker, A. Wysoker, T. Fennell, J. Ruan, N. Homer, G. Marth, G. Abecasis, R. Durbin, The Sequence Alignment/Map format and SAMtools, *Bioinformatics* **25**, 2078–2079 (2009).

18. S. Anders, P. T. Pyl, W. Huber, HTSeq-A Python framework to work with high-throughput sequencing data, *Bioinformatics* **31**, 166–9 (2015).

19. M. I. Love, W. Huber, S. Anders, Moderated estimation of fold change and dispersion for RNA-seq data with DESeq2, *Genome Biol.* **15**, 1–21 (2014).

20. M. E. Ritchie, B. Phipson, D. Wu, Y. Hu, C. W. Law, W. Shi, G. K. Smyth, Limma powers differential expression analyses for RNA-sequencing and microarray studies, *Nucleic Acids Res.* **43**, e47 (2015).

21. A. Federico, S. Monti, HypeR: An R package for geneset enrichment workflows, *Bioinformatics* **36**, 1307–8 (2020).

22. A. A. Sergushichev, An algorithm for fast preranked gene set enrichment analysis using cumulative statistic calculation, *bioRxiv* , 060012 (2016).

23. W. Luo, C. Brouwer, Pathview: An R/Bioconductor package for pathway-based data integration and visualization, *Bioinformatics* **29**, 1830–1 (2013).

24. L. Gatto, K. S. Lilley, Msnbase-an R/Bioconductor package for isobaric tagged mass spectrometry data visualization, processing and quantitation, *Bioinformatics* **28**, 288–9 (2012).

25. G. K. Smyth, in *Bioinformatics and Computational Biology Solutions Using R and Bioconductor*, (Springer New York, New York, NY, 2005), pp. 397–420.

26. K. De Bock, M. Georgiadou, S. Schoors, A. Kuchnio, B. W. Wong, A. R. Cantelmo, A. Quaegebeur, B. Ghesquière, S. Cauwenberghs, G. Eelen, L. K. Phng, I. Betz, B. Tembuyser, K. Brepoels, J. Welti, I. Geudens, I. Segura, B. Cruys, F. Bifari, I. Decimo, R. Blanco, S. Wyns, J. Vangindertael, S. Rocha, R. T. Collins, S. Munck, D. Daelemans, H. Imamura, R. Devlieger, M. Rider, P. P. Van Veldhoven, F. Schuit, R. Bartrons, J. Hofkens, P. Fraisl, S. Telang, R. J. Deberardinis, L. Schoonjans, S. Vinckier, J. Chesney, H. Gerhardt, M. Dewerchin, P. Carmeliet, Role of PFKFB3-driven glycolysis in vessel sprouting, *Cell* **154**, 651–63 (2013).